Electrical Engineering Undergraduate Honors Theses

Electrical Engineering

Development of Intermediate Band Solar Cell through InGaN Quantum Well Structures

Kelly McKenzie
University of Arkansas, Fayetteville

Citation

McKenzie, K. (2017). Development of Intermediate Band Solar Cell through InGaN Quantum Well Structures. *Electrical Engineering Undergraduate Honors Theses* Retrieved from https://scholarworks.uark.edu/eleguht/52

Development of Intermediate Band Solar Cell through InGaN Quantum Well Structures

A thesis submitted in partial fulfillment
of the requirements for the degree of
Honors Studies in Electrical Engineering

by

Kelly Elizabeth McKenzie

May 2017
University of Arkansas

Table of Contents

List of Figures

List of Tables

Abstract

In the search for high-efficiency solar cells, $In_xGa_{1-x}N$ has come under scrutiny as a unique material with high potential. This is due to characteristics including an easily tunable bandgap, large range of potential bandgap values, and high heat resistance. However, one factor limiting its adaptation is the high density of crystal defects. In this thesis, the qualities of InGaN are discussed and the intermediate band solar cell structure is introduced. Additionally, the growth and characterization of two sets of InGaN-based solar cell devices are reported and evaluated.

Acknowledgments

Thank you to Dr. Ware, without whom none of this would be possible. Thank you also to everyone who shared their valuable time to teach me about and aid me with growth and data collection, including Yang Wu, Saeed Sarollahi, Andrian Kuchuk, and especially Pijush Ghosh. And of course, thanks Mom.

1. Introduction

1.1 Overview

Development of single junction silicon solar cells has reached a level where further increase in efficiency is expected to be minimal. Novel materials and device structures must be established if we are to break past the single junction theoretical maximum efficiency of ~30% [1]. $In_xGa_{1-x}N$ is a relatively new, promising material that offers an easily tunable bandgap, which spans in energy more than the entire visible solar spectrum and can therefore be matched to the ideal energies for multi-junction solar cell designs or simply to the ideal single junction bandgap energy. This direct bandgap material also offers high carrier mobility, high absorption coefficient, and high resistance to heat [2]. These qualities make it very useful in a variety of solar cell designs.

However, the lattice mismatch between indium nitride and gallium nitride and between these and sapphire, the most common substrate, means that crystal defects are very common and inhibit the success of devices based on this material. Use of InGaN is also hampered by the difference in vapor pressure between indium and gallium, which makes it difficult to incorporate the large amount of indium necessary to reach lower bandgaps. New solar cell designs may provide a way around this problem. One novel design which has shown promise for InGaN is the intermediate band solar cell, offering a maximum theoretical efficiency of 63% [3].

1.2 Thesis Statement

The goal of this thesis is to fabricate solar cells based on InGaN that employ an intermediate band created using a quantum well superlattice. These devices will be characterized to determine their applicability for energy production and to suggest future improvements in the structure.

1.3 Approach

This thesis will discuss the physical qualities and considerations pertaining to InGaN. It will also discuss intermediate band solar cells and how these offer solutions to the problems inherent to the material. Finally, the paper will detail the growth of an n-GaN/InGaN/p-GaN p-n junction structure and an intermediate band structure based on a quantum well superlattice by molecular beam epitaxy and report the characterization of the resulting devices.

1.4 Organization of the Thesis

The thesis is organized as follows: First, the background of the topic will be introduced in Chapter 2, including a discussion of fabrication and characterization techniques. Next, the experimental details will be provided in Chapter 3. The results of the work will be given in Chapter 4 and conclusions will be drawn in Chapter 5. Finally, references will be provided in Chapter 6.

2. Background

2.1 Photovoltaics

The photovoltaic effect, the creation of a voltage in a material when exposed to light, was first discovered in 1839 by Edmond Becquerel [4]. The first true solar cell was created fifty years later by Charles Fritts, and the first silicon-based device, known at the time as a solar battery and exhibiting a power efficiency of only 6%, was created by Daryl Chapin and some of his associates at Bell Telephone Laboratories in 1945. Since this time, dramatic improvements have been made. It took less than ten years to achieve 14% efficiency, and now commercial silicon single junction solar panels, aided by the optimization of silicon processing techniques for the production of electronics, easily offer power efficiencies averaging 16% [5]. However, the thermodynamic efficiency limit for these devices is only about 30%. If higher efficiencies are desired, different technologies must be employed.

One key technique for increasing solar cell efficiency is bandgap matching. Two of the main losses in solar cells are transmission of low-energy light and thermalization of high-energy light [6]. For example, the bandgap of silicon is about 1.1eV, which corresponds to light in the near-infrared with a wavelength of 1100nm. In this case, any light of wavelength higher than 1100nm will pass through the solar cell without being absorbed. All light above 1100nm will be absorbed by the device. However, the excess energy of this light above 1.1eV will be lost as heat because the electrons relax to the lowest available energy level in a process called thermalization. Silicon's bandgap is very close to the ideal single junction bandgap, but solar cell efficiencies can be pushed even higher when materials with multiple bandgaps are used to absorb different ranges of the solar spectrum more efficiently.

2.2 InGaN

$In_xGa_{1-x}N$, a semiconductor alloy of variable composition, is a promising material for solar cells that offers multiple benefits, as described in Ref. [2]. First, the electronic bandgap can be tuned by changing the In:Ga ratio and can be varied from GaN's 3.4eV to InN's 0.64eV. InGaN is particularly useful as one of the few semiconductor materials that can provide a bandgap above 2.4eV, which is necessary for use in high-efficiency systems with four or more junctions [2]. The wide bandgap also gives it high resistance to heat, unlike silicon devices that experience efficiency loss when heated by sunlight. It has a direct bandgap, high carrier mobility, and high absorption coefficient, all of which suggest that InGaN has the potential to create the next generation of solar cells.

However, it is difficult to incorporate large amounts of indium into the material while maintaining a high crystal quality. Lattice mismatch between GaN and InN, shown in Table 1, and differences in vapor pressure lead to crystal defects which form during growth, including dislocations and phase separation [7]. As the diagrams in Figure 1 demonstrate, materials with the same lattice constant will fit together without strain (a). However, materials with different lattice constants (b) will not necessarily form high-quality crystals. In small amounts of material, the lattice may remain strained to the substrate as in (c), where the lattice is stretched or compressed to match that of the substrate. If too much stress is applied
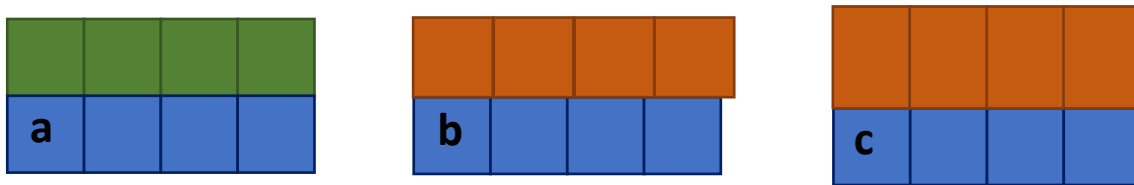

Figure 1. (a) Lattice matched crystal. (b) Lattice mismatched crystal. (c) Strained lattice mismatched crystal.

though, such as if the mismatched layer is grown beyond a certain critical thickness, the crystal will relax by breaking apart and creating defects.

These difficulties currently limit the broad adaption of this material. However, a new concept for solar

cell design offers the potential to alleviate these defects while increasing efficiency compared to standard

single junction devices.

Table 1. Comparison of InN and GaN [8].

Characteristic	Indium Nitride	Gallium Nitride
Bandgap (E_g)	0.64eV, direct	3.4eV, direct
Lattice Constant	a = 3.545 Å, c = 5.703 Å	a = 3.189 Å, c = 5.185 Å
Crystal Structure	Wurtzite	Wurtzite
Thermal expansion coefficient	$\alpha^\perp = 4 \times 10^{-6}/K$, $\alpha^{||} = 3 \times 10^{-6}/K$	$\alpha^\perp = 4.91 \times 10^{-6}/K$, $\alpha^{||} = 4.05 \times 10^{-6}/K$

2.3 Intermediate Band

In intermediate band solar cells (IBSCs), an intermediate band (IB) is introduced between the valence (VB)

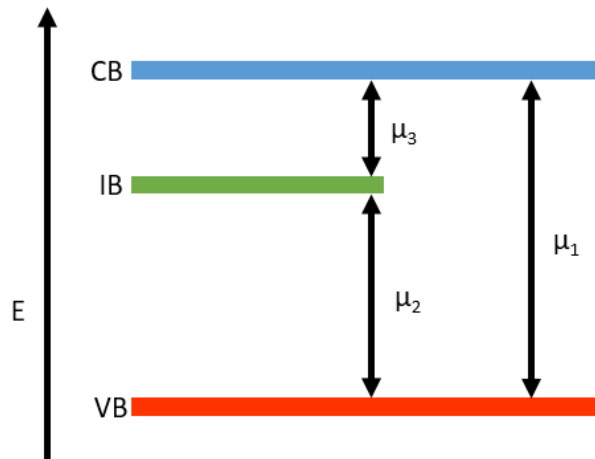and conduction (CB) bands of the device, as shown in Fig. 2.

Figure 2. Electron transitions in IB solar cell.

Photons with energy greater than the bandgap can still excite electrons directly from the VB into the CB.

Subbandgap photons with lower energy than the bandgap, normally lost due to lack of absorption, can

excite electrons from the VB to the IB, and from the IB to the CB. This two-step process allows both low- and high-energy photons to be more fully utilized, maintaining the open-circuit voltage (V_{oc}) due to the bandgap of the nominally wider bandgap material, shown in Fig. 2 as μ_1, while increasing the number of electrons excited in order to generate a short-circuit current (I_{sc}) comparable to that of a smaller bandgap material [9]. The theoretical maximum efficiency for these devices has been predicted to be 63% [10], which is higher than the theoretical efficiency limit for a four-junction tandem device [2].

One approach to creating an intermediate band solar cell is to use nanostructures within the active region of a device, creating "traps" of low-bandgap material that allow low energy electron wavefunctions to overlap, creating an isolated IB that gives electrons a lower energy storage level between the VB and CB [11]. Quantum wells (QWs) are currently one of the most predictable and controllable methods of creating nanostructures. The growth methods, usually utilizing chemical vapor deposition or molecular beam epitaxy, are well established [12]. The bandgaps can be easily tuned by adjusting the material composition and the thickness of the QWs. InGaN QW superlattices can be utilized to create IBs by alternating periods of high indium content wells with low indium content barrier layers. Using thin high indium content layers instead of a single thick absorber layer also helps to reduce stress-related defects associated with the InGaN alloy.

Research into IB devices is still relatively new, but it has grown from the original concept of the IB in 1997 [10] through the development of quantum dot (QD) IBSCs [13] with further enhancement via high QD density and strain compensation [14]-[16], and most recently with hybrid QD/quantum well IBSCs [17] and quantum wire IBSCs [18]. However, the devices that have been tested are still far below the predicted efficiency limit. The resulting V_{oc} is much lower than that of control devices, which has been explained by the effective decrease in the bandgap that results from the IB and CB overlapping and by a VB offset

created by the QWs. The I_{sc} also has not been observed to increase as predicted by theory, which has nominally been explained to be due in part to defects [11] and suboptimal QW design [12].

2.4 Fabrication

2.4.1 Molecular Beam Epitaxy

For this project, the samples were grown using a Veeco Gen II Molecular Beam Epitaxy (MBE) system. MBE systems function by heating elements such as gallium, indium, magnesium, or silicon and varying their vapor pressure in a controlled environment. The gaseous elements are sent across a vacuum chamber containing the substrate where they condense, reacting with each other on the substrate. The ultra-high vacuum utilized in the process allows for the fabrication of incredibly pure materials with precise control of the composition down to layers of single atom thickness.

The substrates used were sapphire with an unintentionally doped GaN (0001) template, purchased from KYMA Technologies [19]. The lattice constant of sapphire is much higher than that of GaN, at a = 4.758 Å [8]. This results in a defect density on the order of $10^8/cm^2$ in the GaN template. These wafers also include a layer of aluminum nitride, used as a nucleation layer for the GaN template. Titanium is applied to the back surface of the wafer to aid in radiative heating of the substrate during growth.

2.4.2 Processing

After growth and optical measurement, samples must be processed into test devices for electrical measurement. First, they are cleaned in HCL for 15 minutes to remove excess Ga droplets from the surface. After cleaning in acetone, methanol, and DI water, AZ4330 photoresist is spin coated at 3000rpm and soft baked at 90°C for 90s. It is then exposed under UV light for 16s for patterning and developed in AZ300MIF developer, and then hard baked at 90°C for 30s.

The test mesas are dry etched using a Plasma-Therm ICP-RIE system and chlorine and boron trichloride gasses which are excited to a plasma in a vacuum chamber. This etch produces cylindrical mesas in the sample of height 700nm and diameters ranging from 300-1100μm.

Contacts are then applied to the sample. After etching in buffered HF to remove surface oxide layers, ohmic contacts are applied via electron beam (e-beam) evaporation. The contacts to the n-type GaN surface consist of Ti (25nm)/Al (100nm)/Ni (50nm)/Au (200nm), annealed at 800°C. The contacts to the p-type GaN surface are Ni (20nm)/Au (20nm)/Ni (20nm)/Au (200nm) without annealing.

2.5 Characterization

2.5.1 Reflectance and transmission

The reflectance and transmission measurements provided in this thesis were taken using a Shimadzu UV-3600 Spectrophotometer. In these measurements, the sample is illuminated with a range of wavelengths from a light source. The UV-3600 can produce any wavelength ranging from ultraviolet at 190nm to near infrared at 3300nm. A detector records the amount of light that is either reflected off or transmitted through the sample, depending on the type of measurement being taken. The coating of titanium on the back of the wafers means that for reflection measurements, incident light will pass through the crystal, reflect off the titanium, and pass back through the crystal, creating what is effectively a two-pass transmission measurement. However, traditional transmission measurements cannot be completed with this coating. The titanium on NJ53 was etched away using buffered oxide etch (BOE), allowing transmission measurements to be completed. Reflectance and transmission results for this sample are provided in Section 4.1. However, this was not done for NJ97, and thus only reflectance measurements are reported.

These measurements can be used to indicate the bandgaps present in the crystal. At low wavelengths, all of the incident light is above the bandgap energy, so the light will be absorbed. This results in very low transmission/reflectance. As the wavelength drops below each bandgap, less and less of the light is absorbed, and therefore a higher transmission/reflection will be recorded. The bandgaps can be identified by noting the wavelength at which there is a strong increase in the transmission.

2.5.2 X-Ray Diffraction

The x-ray diffraction (XRD) measurements in this project are measured with a Philips X'Pert MRD diffractometer. An x-ray beam is reflected off the sample and into a detector. Diffraction patterns are created by the interference of beams reflecting off atoms in different planes of the crystal. When the beams reflecting off atoms in parallel planes of the crystal interfere constructively, a peak is created. For rocking curve measurements, the angle of the sample relative to the incident beam is changed in order to scan the crystal lattice, and the angles where peaks are located are indicative of the lattice spacing of the atoms producing the peak. Therefore, the peak angle can be used to identify the composition of the crystal. The results of these measurements are provided in Section 4.2.

A reciprocal space map of the crystal can also be created with XRD. This two-dimensional image shows bright peaks when large amounts of the crystal correspond to the same lattice constants in two directions. For crystals where lattice mismatch is a concern, this can be used to indicate whether the crystal is still strained to the substrate or if it has relaxed. If peaks are aligned with each other such that they have the same lattice constant (ie, if they are vertically aligned), then they have same lattice constant and the crystal is strained to the substrate. Otherwise, part of the crystal has a different lattice constant and therefore has relaxed, creating defects.

2.5.3 Atomic Force Microscopy

The surface morphology of the crystal was obtained via atomic force microscopy (AFM) using a Bruker Dimension 3000 AFM in tapping mode. A silicon cantilever with a 10nm radius of curvature was used to sweep across the surface of the crystal and measure surface features. The pendulum swing of the cantilever sometimes results in artifacts in the data such as the appearance of dark valleys at the edges of the images. These can be flattened in software such as WSxM to recover the true data. AFM measurements are provided in Section 4.3.

2.5.4 Photoluminescence

In photoluminescence (PL) measurements, a high-energy laser beam is incident on the sample to excite electrons above the bandgap energy. After being excited, these electrons recombine and emit light corresponding to the bandgap of the crystal. In this project, the PL of the crystal was excited with ~1mW emission from a 325nm He-Cd laser, collected and dispersed in a 0.5 meter focal length spectrometer, and detected with a liquid nitrogen-cooled silicon CCD detector. The sample was cooled using a closed cycle helium cryostat to avoid thermal effects in the emission, where electronic transitions are less likely to occur through emission of light than they are to occur through scattering off of lattice vibrations. PL measurements are provided in Section 4.4.

2.5.5 Current-Voltage

The primary method of electrical characterization of solar cells is the measurement of current-voltage (IV) curves. The device is swept with a bias voltage and the resulting current is measured. As a solar cell is simply a type of diode, this will result in a standard diode curve when the cell is in darkness, and the data

is known as the dark IV curve. When the cell is illuminated, the diode curve shifts downward due to the increase in charge carriers and is called the light IV curve.
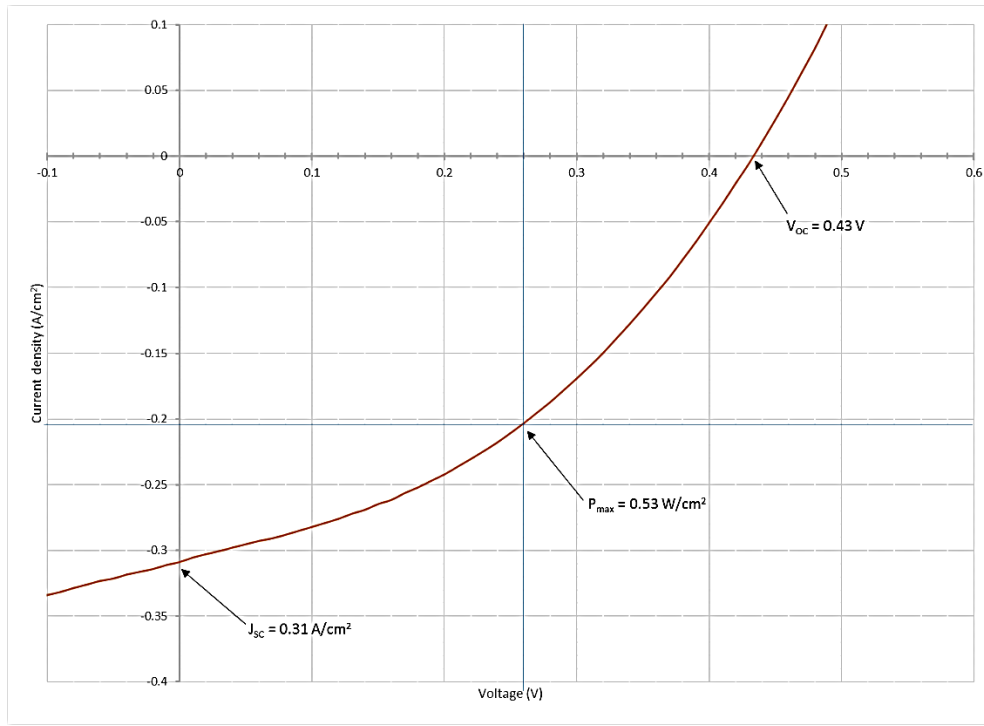

Figure 3. Example light IV curve.

Figure 3 shows an example light IV curve for a hypothetical solar cell. The intersection of the curve with the y-axis gives the short-circuit current density (J_{OC}) of the device, when the voltage between the two contacts is zero and current output is at its maximum. The intersection with the x-axis gives the open-circuit voltage (V_{OC}), where the current output is zero and the voltage between the contacts is at its maximum.

This curve can be used to identify several important characteristics of the device. Between the J_{SC} and V_{OC} lies the maximum power point of the cell, the current-voltage combination that provides the most output power. The fill factor (FF) of the cell is found by dividing the maximum power by the product of V_{OC} and J_{SC}. The power efficiency (η) of the cell is found by dividing the maximum power by the input power to the solar cell, traditionally the one-sun power 100 mW/cm^2.
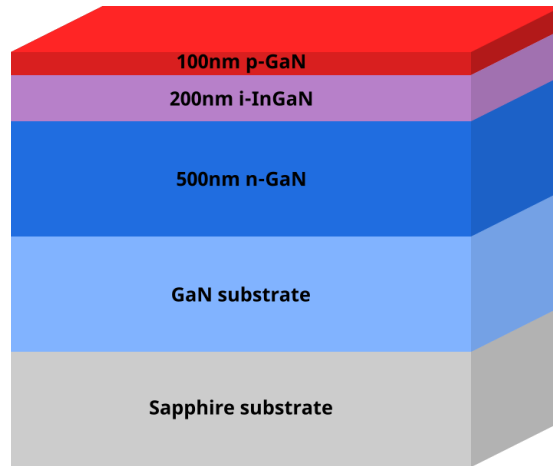
17

3. Experiment

Figure 4. NJ53 crystal structure.

Two different solar cells were fabricated. A p-GaN/InGaN/n-GaN device, identified as NJ53, was designed using Ref. [20] as a guideline, and is shown in Fig. 4. This device was intended to be used as a control by which to compare the characteristics of an intermediate band device. 500nm layer of n-type GaN using Si as a dopant was grown on the GaN template wafer. This layer was grown in three rounds of 200nm, 200nm, and 100nm with the substrate held at 800°C in order to allow for desorption of excess Ga during the growth. This was followed by a 200nm layer of nominally $In_{0.2}Ga_{0.8}N$, grown with the substrate at 600°C. The structure was capped with 100nm of p-type GaN using Mg as a dopant, also grown at 600°C. These relatively low growth temperatures were chosen to allow for better incorporation of In and Mg into the crystal, given the tendency for phase separation of InN and GaN at high temperatures [7].

An intermediate band device, identified as NJ97, was also fabricated. Structure details are provided in Fig. 5. The structure was chosen to be symmetric to NJ53 but to contain a quantum well superlattice instead of the bulk InGaN absorber layer. The well layers were designed to contain 30% indium while the barrier layers were designed to contain 20% indium. The well and barrier thicknesses were chosen as 2nm and 3nm, respectively, based on the recommendations in Refs. [21] and [22]. 24 periods of

superlattice were grown, capped at either end with 40nm of $In_{20}Ga_{80}N$ to prevent tunneling of low-energy

electrons. The n-type GaN was grown at 800°C, and the remainder of the crystal was grown at 600°C.

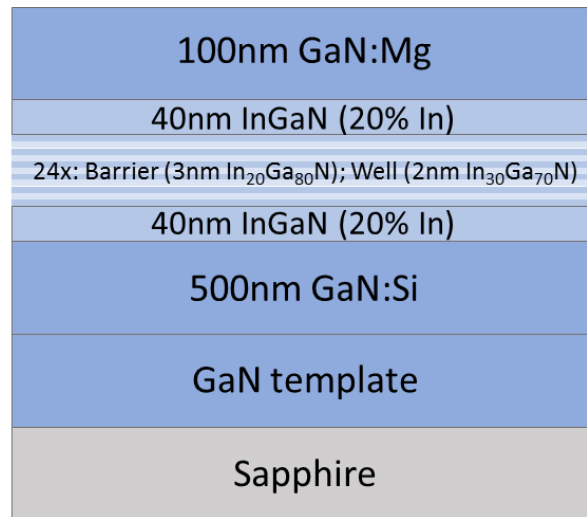| 100nm GaN:Mg |
| 40nm InGaN (20% In) |
| 24x: Barrier (3nm $In_{20}Ga_{80}N$); Well (2nm $In_{30}Ga_{70}N$) |
| 40nm InGaN (20% In) |
| 500nm GaN:Si |
| GaN template |
| Sapphire |

Figure 5. NJ97 crystal structure.

4. Results

4.1 Reflectance and Transmission

The reflectance and transmission of the two samples were measured as described in Section 2.5. The results are given in Figure 6. The raw data for the two samples is shown by the black and red curves. Derivatives of these curves are shown in blue and magenta and are used to more precisely indicate features in the data.
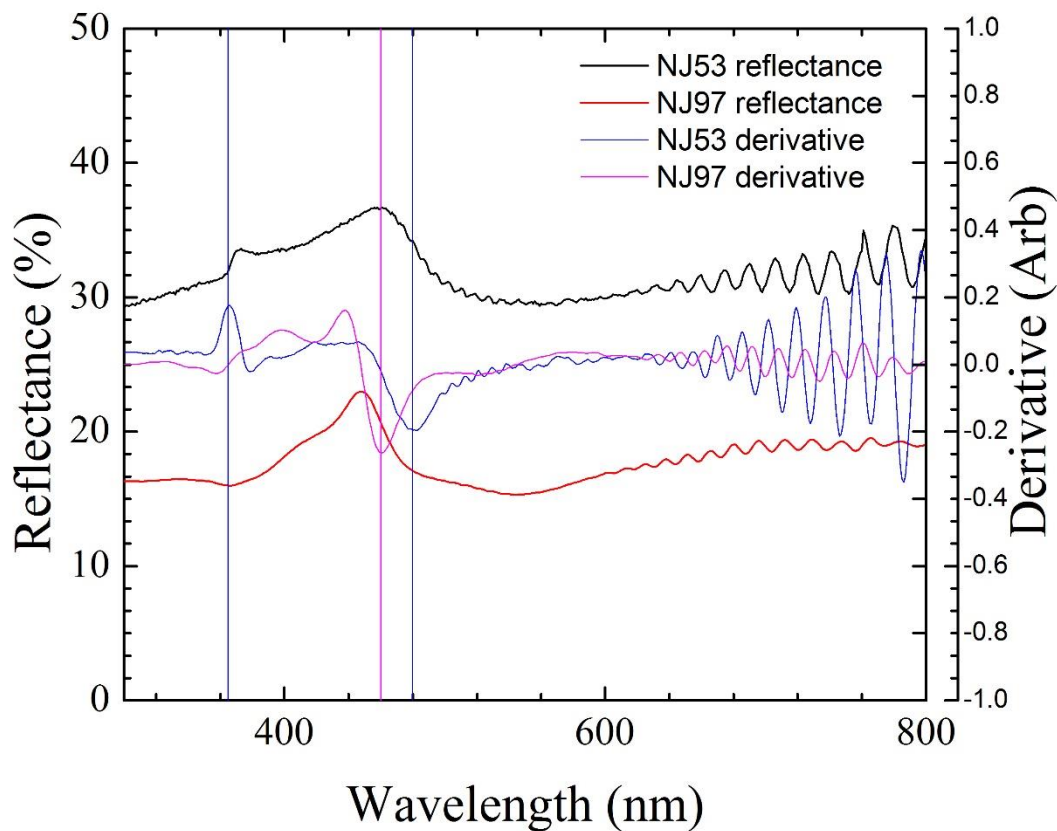

Figure 6. Reflectance and derivatives of reflectance.

Three vertical lines are drawn on the graph. The two blue lines correspond with the data for NJ53 and indicate two major peaks (local minima and maxima) in the derivative of the reflectance curve. The first line at 366nm marks the features corresponding to GaN bandgap, 3.4eV, in the sample. This also indicates the same features in the NJ97 data. The second line at 480nm marks the InGaN bandgap, corresponding

to 2.6eV. The line in magenta indicates InGaN in NJ97 at 460nm, which corresponds to 2.7eV and suggests a slightly lower indium content than NJ53.

For comparison, Figure 7 shows an overlay of the reflectance, derivative of the reflectance, and the more traditional transmission data for NJ53. The two vertical lines again indicate the GaN features in the three curves at 366nm and InGaN features at 480nm. The features indicated by slopes in reflectance and transmission measurements are more clearly seen with the peaks in the derivative of the reflectance.
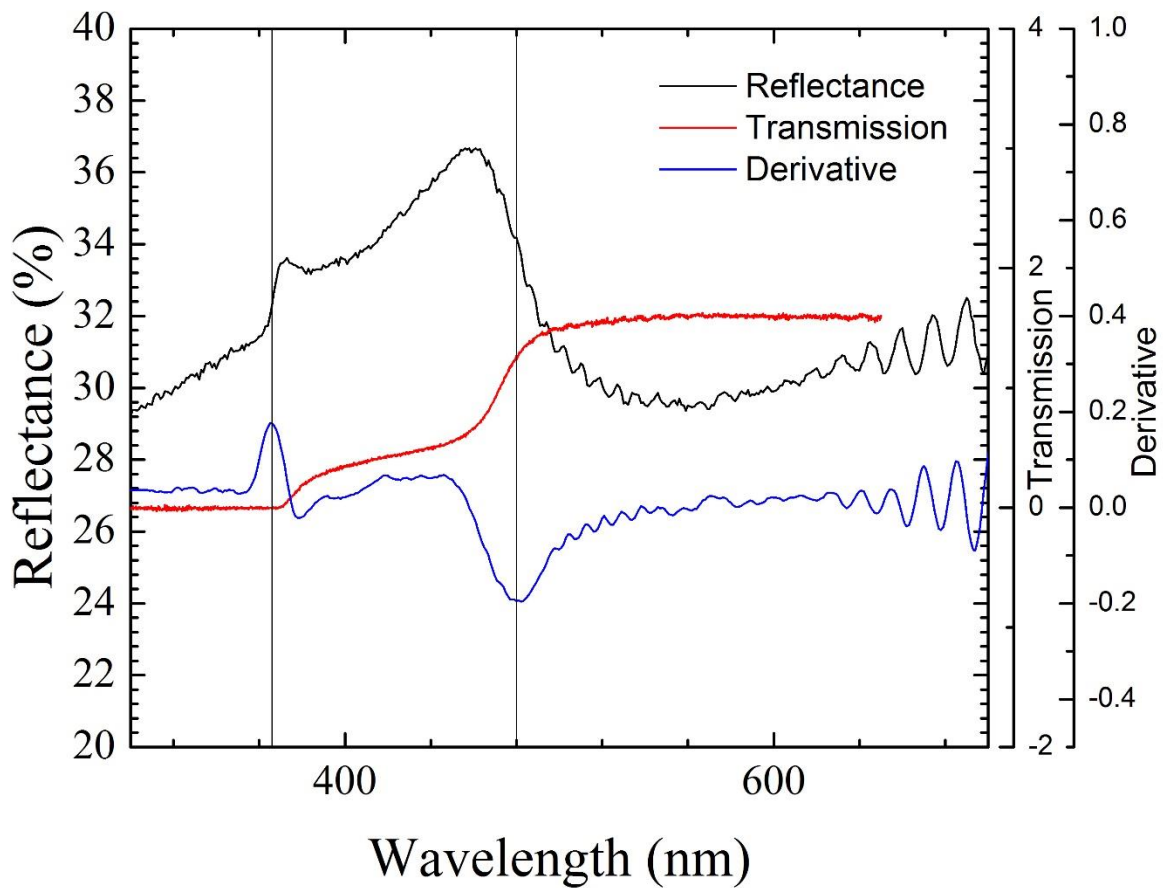

Figure 7. Reflectance, derivative of reflectance, and transmission of NJ53.

The precise bandgaps of InGaN in NJ97 are difficult to discern due to the complex superlattice structure.

Many of the oscillations in the graph, especially those visible past 500nm, are due to thin-film interference

fringes, and these likely cause some of the fluctuations in the 300-500nm range as well. However, a lower

bandgap InGaN feature may be observable at 520nm in Fig. 6, suggesting a bandgap in the wells of 2.38eV.

4.2 X-Ray Diffraction

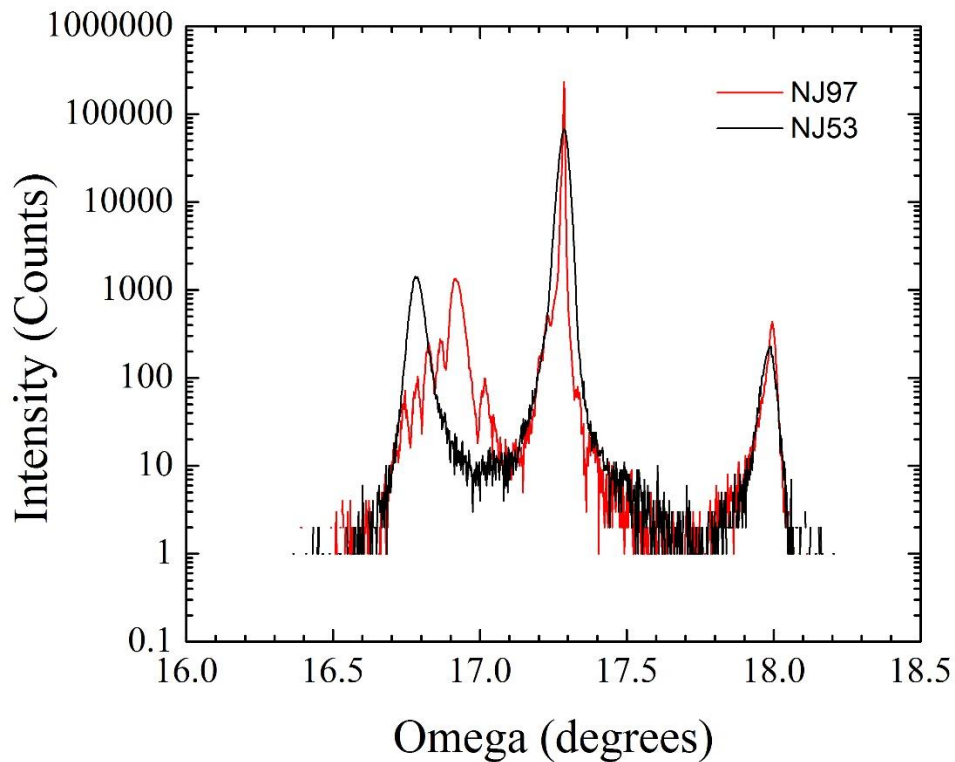The XRD rocking curves for NJ53 and NJ97 are shown in Figure 8.

Figure 8. XRD rocking curves of NJ53 and NJ97.

The rightmost peaks indicate aluminum nitride present in the purchased substrates. The center peaks

indicate GaN, and the leftmost peaks indicate InGaN. The position of the NJ53 InGaN peak indicates that

the indium concentration in that sample is 18.5%, very close to the designed 20%. The NJ97 InGaN peak

shows thin-film interference fringes which indicate the presence of a superlattice, but making the

determination of the indium concentration within the superlattice is not possible analytically and is

beyond the scope of this work. However, the position of the main peak at higher angles than the NJ53

peak, combined with the reflectance data, suggests again that some of the InGaN has a lower indium

concentration and therefore higher bandgap than NJ53.

22

4.3 Atomic Force Microscopy

Representative AFM images of the two samples are shown below.
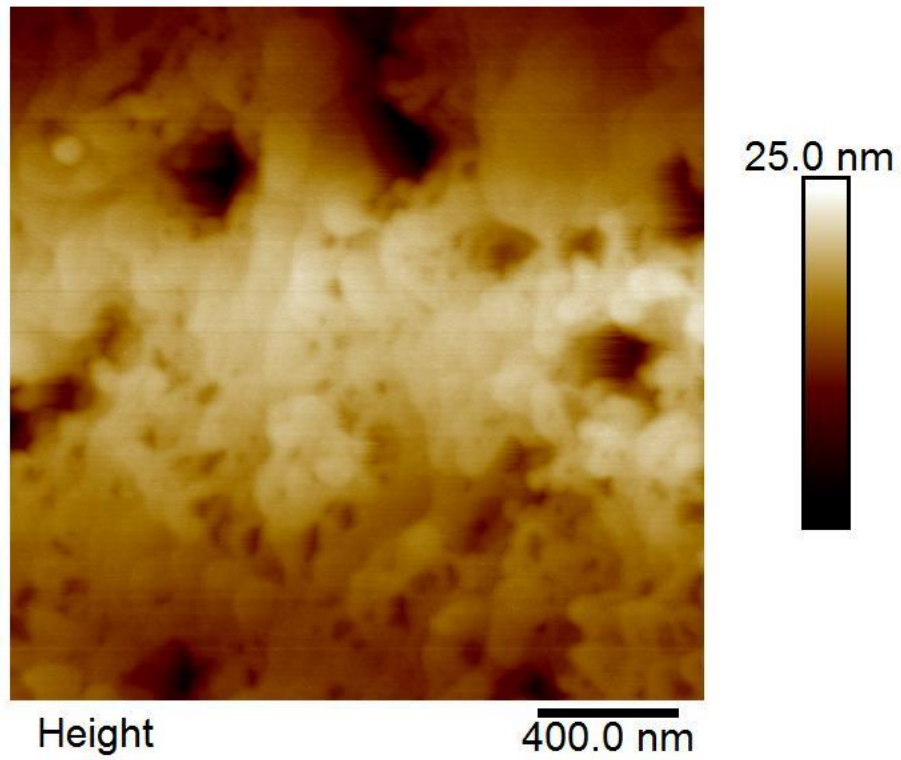

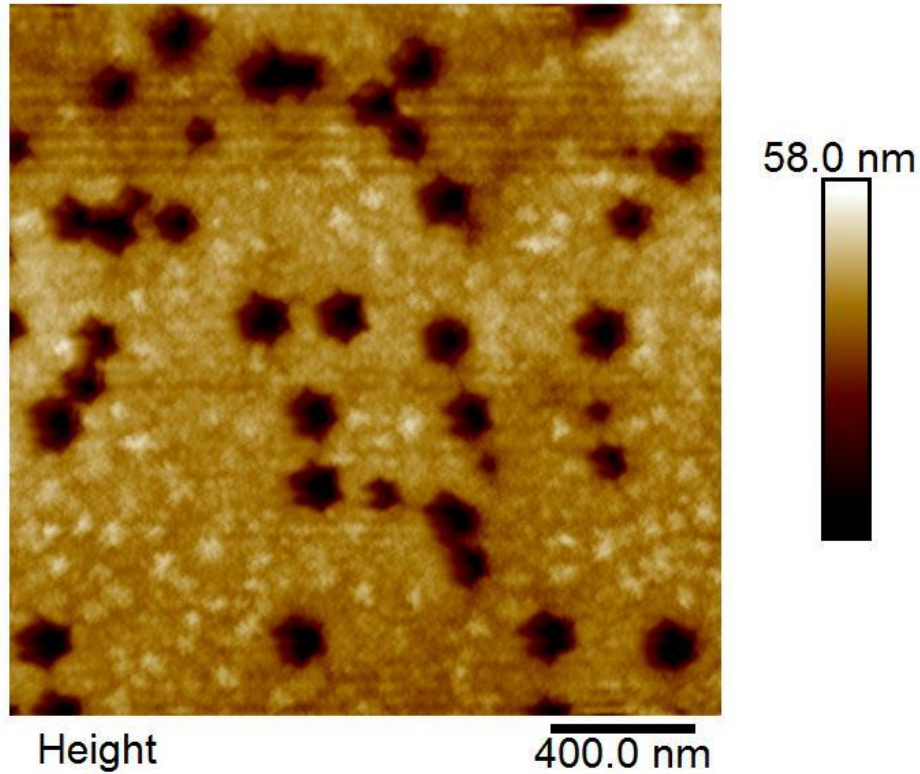Figure 9. AFM image of NJ53 surface.

Figure 10. AFM image of NJ97 surface.

The surfaces are quite smooth, with the exception of small holes. These are likely the result of threading dislocations in the crystals. As reported in Section 2.4.1, the dislocation density of the GaN template on the purchased substrate wafer is approximately $10^8/cm^2$, or one per square micron, which matches the density observed in NJ53. The number density in NJ97 is closer to 10 per square micron, which is higher but not unreasonable.

4.4 Additional NJ53 Data

The photoluminescence of NJ53, taken at a temperature of 15K, is shown in Figure 11. The small peak at 358nm is due to emission from the GaN. The peak at 482nm indicates InGaN. These results closely match the reflectance data.
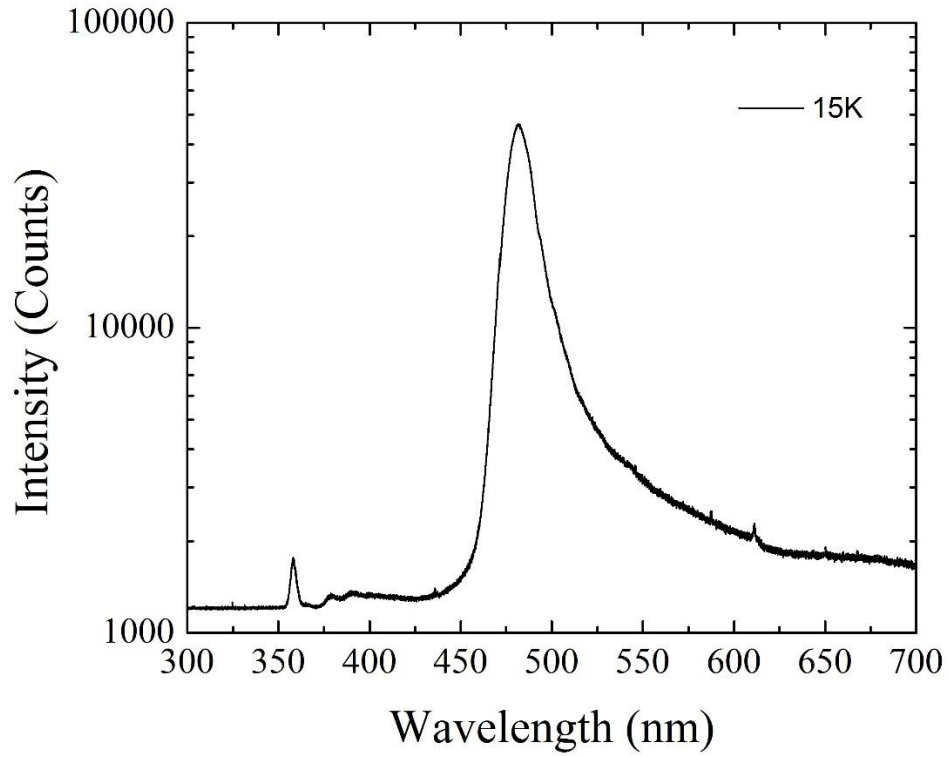
Figure 11. Log scale PL spectra of InGaN p-n crystal.

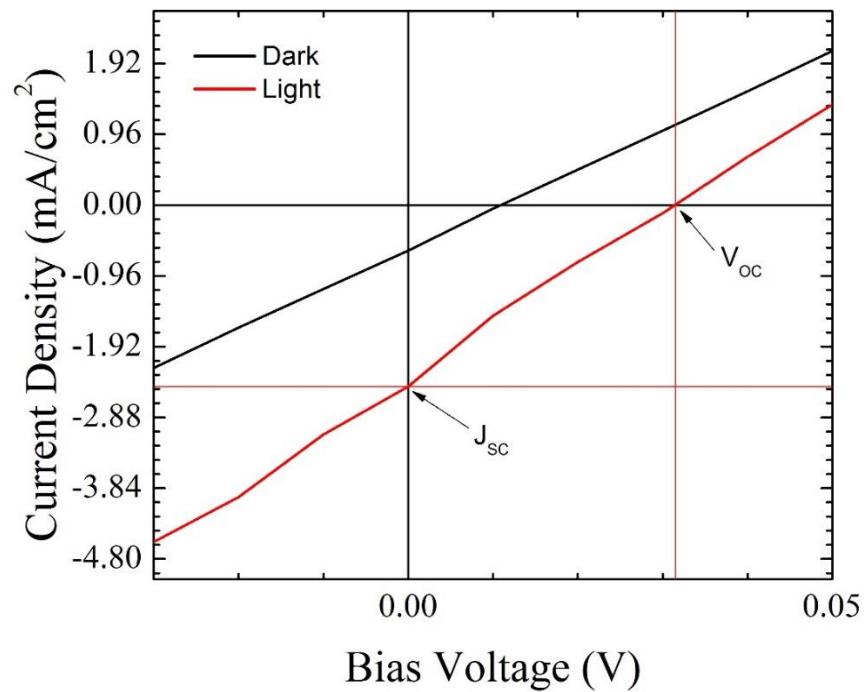The current-voltage characteristics of NJ53 are given below.

Figure 12. Current-voltage characteristics of NJ53.

The open-circuit voltage and short-circuit current density are indicated in the figure by labels and by horizontal and vertical lines. The measured V_{OC} is 0.03V, and J_{SC} is 2.46mA/cm^2. The maximum power point of the sample is 1.1×10^{-5}mW. This results in a fill factor of 21% and a power efficiency of 0.015%. These numbers are quite low and may be attributed to a number of causes, including shading from the top contact and inadequate p-type doping.

Final optical and electrical measurements of NJ97 are the topic of ongoing work. These results demonstrate that the reference sample structure will need to be modified in order to make a viable comparison with the intermediate band device; however, these initial attempts provide promising optical and structural results.

5. Conclusion

5.1 Review of Thesis

In$_x$Ga$_{1-x}$N is a novel semiconductor material that offers a variety of benefits for solar cell design including an easily tunable bandgap with the ability to reach bandgaps in almost the full range between 0.6eV and 3.5eV. Development has been hindered by the high density of crystal defects due to lattice mismatch between indium nitride and gallium nitride and between these and the most common substrate, sapphire. New solar cell designs such as intermediate bands based on quantum well superlattices may reduce the amount of indium required and therefore the stress-related defects in the crystal.

Two InGaN solar cells were grown via MBE, a control device with a bulk In$_{20}$Ga$_{80}$N absorber layer and an intermediate band device with 24 periods of quantum wells. Optical characterizations of the devices

indicate promising results that can be used in the future to refine the structures and achieve high-efficiency InGaN solar cells.

5.2 Future Work

Additional optical and electrical characterization, particularly PL and IV, is the subject of future work on NJ97. Another control device will need to be designed and fabricated in order to produce higher quality electrical results than NJ53, with suggestions including increasing the Mg doping of the p-type GaN layer and choosing a different style of contacts that produce less shading of the cell. Depending on the results obtained from NJ97, potential areas for improvement include increasing the indium content of the superlattice to decrease the bandgap, increasing the number of periods in the superlattice to increase light absorption, and increasing the p-type doping.

6. References

[1] W. Shockley and H. Queisser, "Detailed Balance Limit of Efficiency of p-n Junction Solar Cells," *Journal of Applied Physics*, vol. 32, no. 3, pp. 510-519, 1961.

[2] A. Bhuiyan, K. Sugita, A. Hashimoto and A. Yamamoto, "InGaN Solar Cells: Present State of the Art and Important Challenges," *IEEE Journal of Photovoltaics*, Vol. 2, No. 3, pp. 276-293, Jul. 2012.

[3] A. Luque and A. Martí, "Increasing the Efficiency of Ideal Solar Cells by Photon Induced Transitions at Intermediate Levels," *Physical Review Letters*, vol. 78, no. 26, pp. 5014-5017, Jun. 1997.

[4] O. Shevaleevskiy, "The future of solar photovoltaics: A new challenge for chemical physics," *Pure and Applied Chemistry*, vol. 80, no. 10, pp. 2079-2089, 2008.

[5] International Energy Agency, "Technology Roadmap: Solar Photovoltaic Energy," Paris, France, 2014.

[6] M. Alam and M. Ryyan Khan, "Fundamentals of PV efficiency interpreted by a two-level model," *American Journal of Physics*, vol. 81, no. 9, pp. 655-662, Jun. 2013.

[7] C. Fabien, B. Gunning, W. Alan Doolittle, A. Fischer, Y. Wei, H. Xie and F. Ponce, "Low-temperature growth of InGaN films over the entire composition range by MBE," *Journal of Crystal Growth*, vol. 425, pp. 115-118, Feb. 2015.

[8] T. Yao and S. Hong, *Oxide and Nitride Semiconductors*, 1st ed. Dordrecht: Springer, 2009, pp. 4-5.

[9] Y. Okada, N. Ekins-Daukes, T. Kita, R. Tamaki, M. Yoshida, A. Pusch, O. Hess, C. Phillips, D. Farrell, K. Yoshida, N. Ahsan, Y. Shoji, T. Sogabe and J. Guillemoles, "Intermediate band solar cells: Recent progress and future directions," *Applied Physics Reviews*, vol. 2, no. 2, p. 021302, Apr. 2015.

[10] A. Luque and A. Martí, "Increasing the Efficiency of Ideal Solar Cells by Photon Induced Transitions at Intermediate Levels," *Physical Review Letters*, vol. 78, no. 26, pp. 5014-5017, Jun. 1997.

[11] A. Luque and A. Martí, "The Intermediate Band Solar Cell: Progress Toward the Realization of an Attractive Concept," *Advanced Materials*, vol. 22, no. 2, pp. 160-174, Jan. 2010.

[12] N. Watanabe, M. Mitsuhara, H. Yokoyama, J. Liang and N. Shigekawa, "Influence of InGaN/GaN multiple quantum well structure on photovoltaic characteristics of solar cell," *Japanese Journal of Applied Physics*, vol. 53, no. 11, p. 112301, Sep. 2014.

[13] A. Martí, N. López, E. Antolín, E. Cánovas, A. Luque, C. Stanley, C. Farmer and P. Díaz, "Emitter degradation in quantum dot intermediate band solar cells," *Applied Physics Letters*, vol. 90, no. 23, p. 233510, Jun. 2007.

[14] K. Yamaguchi and T. Kanto, "Self-assembled InAs quantum dots on GaSb/GaAs(001) layers by molecular beam epitaxy," *Journal of Crystal Growth*, vol. 275, no. 1-2, pp. e2269-e2273, Feb. 2005.

[15] R. Laghumavarapu, M. El-Emawy, N. Nuntawong, A. Moscho, L. Lester and D. Huffaker, "Improved device performance of InAs⁄GaAs quantum dot solar cells with GaP strain compensation layers," *Applied Physics Letters*, vol. 91, no. 24, p. 243115, Dec. 2007.

[16] S. Park, Y. Moon, J. Lee, H. Kwon, J. Park and D. Ahn, "Enhancement of light power for strain-compensated hybrid InGaN/InGaN/MgZnO light-emitting diodes," *Appl. Phys. Lett.*, vol. 97, no. 12, p. 121107, Sep. 2010.

[17] S. Hatch, J. Wu, K. Sablon, P. Lam, M. Tang, Q. Jiang and H. Liu, "InAs/GaAsSb quantum dot solar cells," *Opt. Express*, vol. 22, no. 3, p. A679, Mar. 2014.

[18] V. Kunets, C. Furrow, M. Ware, L. de Souza, M. Benamara, M. Mortazavi and G. Salamo, "Band filling effects on temperature performance of intermediate band quantum wire solar cells," *Journal of Applied Physics*, vol. 116, no. 8, p. 083102, Aug. 2014.

[19] Kyma Technologies, Gallium *Nitride (GaN) Templates,* [Online]. Available: http://www.kymatech.com/products/materials/41-templates/35-gan-templates.

[20] C. Fabien, A. Maros, C. Honsberg and W. Doolittle, "III-Nitride Double-Heterojunction Solar Cells With High In-Content InGaN Absorbing Layers: Comparison of Large-Area and Small-Area Devices," IEEE Journal of Photovoltaics, vol. 6, no. 2, pp. 460-464, 2016.

[21] L. Redaelli, A. Mukhtarova, A. Ajay, A. Núñez-Cascajero, S. Valdueza-Felip, J. Bleuse, C. Durand, J. Eymery and E. Monroy, "Effect of the barrier thickness on the performance of multiple-quantum-well InGaN photovoltaic cells," Japanese Journal of Applied Physics, vol. 54, no. 7, p. 072302, Jun. 2015.

[22] L. Redaelli, A. Mukhtarova, S. Valdueza-Felip, A. Ajay, C. Bougerol, C. Himwas, J. Faure-Vincent, C. Durand, J. Eymery and E. Monroy, "Effect of the quantum well thickness on the performance of InGaN photovoltaic cells," Applied Physics Letters, vol. 105, no. 13, p. 131105, Sep. 2014.